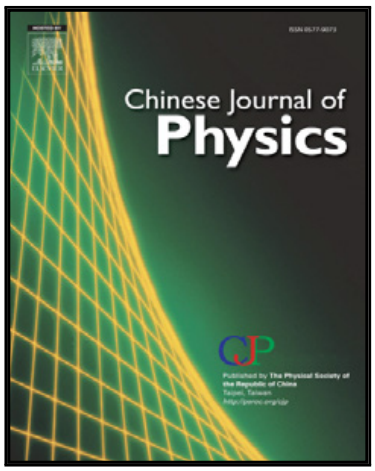

Mathematical model for ciliary-induced transport in MHD flow of Cu-H_2O nanofluids with magnetic induction

Noreen Sher Akbar , Dharmendra Tripathi , Zafar Hayat Khan , O. Anwar Bég

PII: S0577-9073(16)30425-7
DOI: 10.1016/j.cjph.2017.03.005
Reference: CJPH 199

To appear in: *Chinese Journal of Physics*

Received date: 30 July 2016
Revised date: 12 March 2017
Accepted date: 12 March 2017

Please cite this article as: Noreen Sher Akbar , Dharmendra Tripathi , Zafar Hayat Khan , O. Anwar Bég , Mathematical model for ciliary-induced transport in MHD flow of Cu-H_2O nanofluids with magnetic induction, *Chinese Journal of Physics* (2017), doi: 10.1016/j.cjph.2017.03.005

Highlights

- Ciliary induced transport by metachronal beating is discussed.
- The wavelength is considered as very large for cilia induced MHD flow.
- Magnetic Reynolds number is sufficiently large to invoke magnetic effects.
- The physical problem is linearized using transformations.
- Closed-form expressions are presented for the solutions.

Mathematical model for ciliary-induced transport in MHD flow of Cu-H_2O nanofluids with magnetic induction

[*1]Noreen Sher Akbar, [2]Dharmendra Tripathi, [3]Zafar Hayat Khan and **[4]O. Anwar Bég**
[1]DBS&H CEME National University of Sciences and Technology, Islamabad, Pakistan
[2]Department of Mechanical Engineering, Manipal University, Jaipur-303007, India.
[3]Department of Mathematics, University of Malakand Dir (lower) Khyber Pakhtunkhwa, Pakistan
[4] Fluid Mechanics, Mechanical and Aeronautical Engineering, Salford University, Newton Building, The Crescent, Salford, Manchester, M5 4WT, UK.

**Corresponding Author: noreensher@yahoo.com (Noreen Sher Akbar)*

ABSTRACT

Motivated by novel developments in surface-modified, nanoscale, magnetohydrodynamic (MHD) biomedical devices, we study theoretically the ciliary induced transport by metachronal wave propagation in hydromagnetic flow of copper-water nanofluids through a parallel plate channel. Under the physiological constraints, creeping flow is taken into consideration i.e. inertial forces are small compared with viscous forces. The metachronal wavelength is also considered as very large for cilia induced MHD flow. Magnetic Reynolds number is sufficiently large to invoke magnetic induction effects. The physical problem is linearized and exact solutions are developed for the resulting boundary value problem. Closed-form expressions are presented for the stream function, pressure rise, induced magnetic field function and temperature. Mathematica symbolic software is used to compute and illustrate numerical results. The influence of physical parameters on velocity profile, pressure gradient and trapping of bolus are discussed with the aid of graphs. The present computations are applicable to simulations of flow control of in nano-magneto-biomimetic technologies.

Keywords: *Copper-Water Nano Fluid; Metachronal Wave; Magnetohydrodynamics; Magnetic Reynolds Number; Biomimetic Magnetic Propulsion.*

1. INTRODUCTION

Ciliary motion features prominently in numerous biological transport processes. Cilia are slim, microscopic, hair-like structures which protrude from the surface of biological vessels, mammalian cells etc. Dimensions of a single cilium are typically several micrometers in length and less than a single micrometer in width. Important functions associated with cilia include surface energy modification, actuation and heat control. In the human body cilia are present in the renal system, the visual system (non-motile cilia in photoreceptors of the retina), digestive

tract and embryological organs [1,2]. Cilia motility is therefore critical to optimizing many fundamental physiological mechanisms including blood circulation, absorption of nutrients, respiration and reproduction. It has also been observed that when a group of cilia operate together, they generally beat slightly out of phase with respect to the adjacent cilia. This synchronization between beating cilia is called *metachronal coordination*. This leads to the formation of a wave called *metachronal wave* which is recognized to improve the fluid flow due to cilia. In humanoid physiques, cilia dynamics contributes significantly to the impulsion of numerous organic liquids, including the hydrodynamics in the ductility efferentes, transport of ovulatory mucus in the oviduct and the removal of trachea-bronchial mucus in the respiratory track. Defects in cilia motility can lead to numerous human diseases. On the other hand, the fascinating pattern of ciliary motion has been exploited by bio-engineers in the fabrication of artificial cilia for microfluidic applications such as micro-pumps for drug-delivery systems. Multiple studies have been performed to investigate the interactions between cilia and flagella with their environment, resulting in many complex hydrodynamic simulations. Mathematical models of cilia-induced biofluid dynamics are therefore of great relevance in further elucidating the complex characteristics intrinsic to many biological systems.

In recent years there has been an explosion of emerging nano-technologies. Engineering at the nano-scale has intruded into many sectors of engineering, medical sciences and even environmental systems. These liquids were synthesized originally to enhance thermal performance properties of standard working fluids e.g. water, air, oils. They have however been increasingly refined and applied to new fields in medicine, pharmacology, haemotology etc. A lucid review has been given by Salata [3]. Specific applications pioneered for drug delivery by the Langer Group at MIT have been described in Zhang *et al*. [4]. In parallel with clinical developments of nanofluids, significant progress in modelling and simulation has also taken place. This constitutes an important compliment to *laboratory-based nano-technology*. Most simulations have deployed one of two formulations for nanofluid transport, namely the *Tiwari-Das model* or the *Buonjiornio model*. The former results in a modified energy transport equation for nano-scale effects. The latter introduces a separate nano-particle diffusion equation and emphasizes Brownian diffusion and thermophoresis as the principal mechanisms for thermal enhancement. In the context of medical flows, Akbar *et al*. [5] used Buonjiornio's model to investigate analytically the peristaltic hydrodynamics of nanofluids with wall slip effects.

Tripathi and Bég [6] also studied peristaltic propulsion of nanofluids and employed a dual Grashof number formulation to simulate both thermal and nano-particle species buoyancy effects. Mustafa *et al.* [7] obtained both homotopy and MAPLE8 numerical solutions for the effect of wall properties and viscous heating on peristaltic nanofluid flow in a tube. Bég *et al.* [8] used Nakamura finite difference and MAPLE software to study rheological bioconvection in nanofluid boundary layer flow in permeable media as a simulation of near-wall transport in microbial nano-fuel cells. Further investigations of nanofluids in biomedical applications include Anghel and Grumezescu [9] who have demonstrated the excellent bacterial adherence (biofilm) inhibiting characteristics of nanofluid oils in the smart design of novel material surfaces for prosthetic devices. Other analytical articles considering nanofluid dynamics in medicine include Ebaid and Aly [10] for peristaltic flows, Akbar *et al*. [11] for curved tube peristaltic transport of copper nanofluids, Saurin *et al.* [12] for ionic nanofluid bio-lubrication systems (hip joints), Bég *et al*. [13] for swirling mixing systems in nano-biopolymers and very recently Uddin *et al.* [14] for gyrotactic bioconvection in slip Sakiadis flows of nano-polymer sheet manufacturing processes. In the context of cilia hydrodynamics, several studies addressing nanofluid transport have also been communicated. Akbar *et al.* [15] consider carbon nanotube (CNT) nanofluid dynamics in a ciliated tube, deriving analytical expressions for velocity, temperature and pressure gradient for various nano-materials. Akbar *et al.* [16] further studied the metachronal copper-water nanofluid dynamics in a ciliated tube. Munawar et al. [17] reported the time dependent flow and heat transfer over stretching sheet. More recently some more investigations [18-22].

The above studies pertaining to nanofluid flows in medicine have generally neglected magnetohydrodynamics (MHD), namely the interaction of nanofluids with electrical and magnetic fields. However the functionality and adaptability of magnetic nanofluids [23, 24] has been established for over a decade. These particles are designed to interact intelligently with the bio-electro-magnetic fields in the human body or to externally applied magnetic fields. The magnetic nano-particles in stream react to a magnetic force which may be exploited in pharmacological targeting, cell sorting, and magnetite nanoparticles embedded with antibodies for tumor-specific MRI treatments and so on. Strong magnetic flux density attracts magnetized nano-particles. The in-situ monitoring of their performance can be achieved now via selected

area electron diffraction (SAED) and superconducting quantum interference measurement devices (SQUIDs). Different organs of the human body can be more receptive to different types of magnetic nano-particles e.g. rod-like geometries of magnetite nano-particles as opposed to spherical-type nanoparticles have been found to be taken up by Kupffer cells days after vein infusion [24]. The clinical confirmation of magnetic nano-particle performance is a very strong motivation to engineers and scientists for examining theoretically the dynamics of the interaction of these particles with electrically-conducting biological fluid media e.g. blood, plasma etc. *Magneto-bio-nano-fluid dynamics* is therefore emerging as a very rich and rewarding arena for investigation. Sheikholeslami [25] used a Lattice-Boltzmann numerical code to investigate magnetic nanofluid convection in annular gaps under buoyancy effects. Sheikholeslami and Ellahi [26] further studied the three dimensional natural convection of nanofluids under the effects of magnetic field. Some more recent works [27-29] on MHD flow of nanofluids have also been reported. Ferdows *et al*. [30] employed a finite difference algorithm to compute thermal radiative flux, wall mass flux and transverse magnetic field effects on hydromagnetic nanofluid transport in stretching sheet flows. Although these studies have confirmed the significant influence of external magnetic (static) fields on magnetic nano-particle transport in different configurations, they have consistently neglected *electromagnetic induction phenomena*, since generally a very small magnetic Reynolds number has been assumed. This invokes magnetic induction phenomena. Roberts [31] experimentally confirmed the importance of incorporating electromagnetic induction in realistic hemodynamic simulations, presenting one of the first investigations of blood magnetohydrodynamics over four decades ago, based on work at the King's College Hospital, London. Much later magnetic induction phenomena were studied in bio-metallic polymer flows by Bég *et al.* [32] who described in some detail the influence of magnetic Prandtl number and also the magnetic flux distribution associated with magnetic Reynolds number. Further investigations of combined heat transfer and magnetohydrodynamic flow with induction effects were communicated by Ghosh *et al*. [33] with buoyancy present, Ghosh *et al.* [34] for oblique magnetic field and Maxwell displacement current effects and by Zueco and Bég [35] for magnetic induction squeeze film swirl hydrodynamics with Batchelor number effects. The studies [32-35] however did not specifically address *biological applications*, rather they considered respectively electromagnetic propulsion systems (magneto-gas dynamic accelerators) and landing gear systems for astronautical vehicles. However Bhargava *et al.* [36]

did implement the formulations in [32-35] to consider electromagnetic induction phenomena in biomagnetic micro-rheological blood flows in tissue using the Rosensweig ferrohydrodynamic theory and a variational finite element code. They showed that magnetization effects in rheological blood flow can only be properly identified via the inclusion of extra magnetic induction equations. More recently Bég *et al*. [37] have considered surface tension-driven magneto-nanofluid dynamics in stretching sheet biopolymers incorporating the full magnetic induction formulation and deriving extensive numerical solutions with MAPLE and finite element method. Bég *et al*. [38] have also addressed magnetic induction phenomena in biological squeezing hydrodynamics of viscous conducting fluids using Adomian decomposition methods. Some other analyses of biophysical magnetic induction flows include the work of Mekheimer [39, 40] and the articles of Hayat *et al*. [41, 42] which all focus on non-Newtonian peristaltic propulsion.

Motivated by novel developments in electromagnetic ciliated nanoscale biological devices (with applications in biomimetic "surface-controlled" propulsion mechanisms of potential use in biochemical engineering and bio-astronautics), in the present work we address the *application and function of cilia with magnetic induction effects in MHD propulsion of nano-bio-fluids in ciliated vessels*. The governing equations for two-dimensional incompressible magnetized Newtonian nanofluids are transformed via the assumptions of long wave number and low Reynold number i.e. viscous-dominated propulsion. The resulting boundary value problem is solved analytically and closed-form expressions derived for the hydrodynamic and magnetic variables. Extensive colour visualization of flow variables is presented and a parametric study of the influence of the key hydrodynamic, magnetic, nanoscale and biological parameters on velocity, pressure gradient, pressure rise, streamline 5nd induced magnetic field distributions is conducted.

2. CILIARY INDUCED TRANSPORT MODEL

In this study, we adopt the well-known envelope approach where the ciliary tips are assumed to move in *elliptical* paths, illustrated in **Fig. 1** and defined mathematically as follows:

$$\bar{Y} = \bar{f}\left(\bar{Z},\bar{t}\right) = a + a\bar{\varepsilon}\cos\left(\frac{2\pi}{\lambda}\left(\bar{Z} - c\bar{t}\right)\right), \tag{1}$$

$$\bar{Z} = \bar{g}\left(\bar{Z}, \bar{Z}_0, \bar{t}\right) = \bar{Z}_0 + a\bar{\varepsilon}\alpha \sin\left(\frac{2\pi}{\lambda}\left(\bar{Z} - c\bar{t}\right)\right), \tag{2}$$

where a denotes the channel half-width, $\bar{\varepsilon}$ is a measure of the cilia length, λ and c stand for wavelength and wave speed of the metachronal wave, α is a measure of the eccentricity of the elliptical motion and $\bar{Z}_0$ is some reference position of the wall particles.

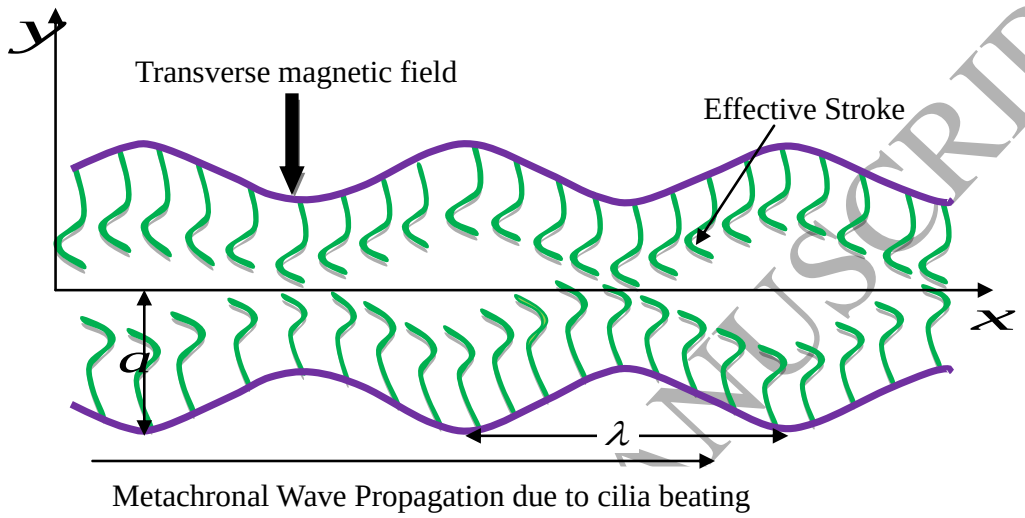

Fig.1. Schematic representation of physical model for MHD flow of nanofluid induced by cilia beating through a channel

If the classical no slip condition is applied at the interior tube walls, then the velocities of the transporting fluid are essentially those induced by the cilia tips, and these may be formulated as follows:

$$\bar{W} = \frac{\partial \bar{Z}}{\partial \bar{t}} = \frac{\partial \bar{g}}{\partial \bar{t}} + \frac{\partial \bar{g}}{\partial \bar{Z}}\frac{\partial \bar{Z}}{\partial \bar{t}} = \frac{\partial \bar{g}}{\partial \bar{t}} + \frac{\partial \bar{g}}{\partial \bar{Z}}\bar{W}, \tag{3}$$

$$\bar{U} = \frac{\partial \bar{R}}{\partial \bar{t}} = \frac{\partial \bar{f}}{\partial \bar{t}} + \frac{\partial \bar{f}}{\partial \bar{Z}}\frac{\partial \bar{Z}}{\partial \bar{t}} = \frac{\partial \bar{f}}{\partial \bar{t}} + \frac{\partial \bar{f}}{\partial \bar{Z}}\bar{W}. \tag{4}$$

Implementing Eqs.(1)&(2) in Eqs.(3)&(4), the velocity components are readily obtained as:

$$\bar{W} = \frac{-\frac{2\pi}{\lambda}\left(\bar{\varepsilon}\alpha a \cos\left(\frac{2\pi}{\lambda}\right)\left(\bar{Z} - c\bar{t}\right)\right)}{1 - \frac{2\pi}{\lambda}\left(\bar{\varepsilon}\alpha a \cos\left(\frac{2\pi}{\lambda}\right)\left(\bar{Z} - c\bar{t}\right)\right)}, \tag{5}$$

$$\bar{U} = \frac{\frac{2\pi}{\lambda}\left(\bar{\varepsilon} a c \sin\left(\frac{2\pi}{\lambda}\right)\left(\bar{Z} - c\bar{t}\right)\right)}{1 - \frac{2\pi}{\lambda}\left(\bar{\varepsilon}\alpha a \cos\left(\frac{2\pi}{\lambda}\right)\left(\bar{Z} - c\bar{t}\right)\right)}, \tag{6}$$

where $\overline{W}$ and $\overline{U}$ be the axial and the radial velocities of the cilia respectively.

3. GOVERNING EQUATIONS

We consider the magnetohydrodynamic (MHD) flow of incompressible Newtonian Cu-H_2O nanofluid through a parallel plate channel, as shown in Fig.1. The inner surface of the channel is flexible and ciliated with metachronal waves and the flow occurs due to collective beating of cilia. An external transverse uniform constant magnetic field H_0 is applied. This generates an induced magnetic field $H\left(h_X\left(\bar{X},\bar{Y},t\right),H_0+h_Y\left(\bar{X},\bar{Y},t\right),0\right)$ and the total magnetic field $H^+\left(h_X\left(\bar{X},\bar{Y},t\right),H_0+H_1+h_Y\left(\bar{X},\bar{Y},t\right),0\right)$ is therefore taken into account. The channel walls are considered to be electrically non-conductive and Hall and Maxwell displacement currents are neglected. The equations governing the conservation of magnetic field, flow and temperature (in the presence of heat source or heat sink) are given, *in vectorial form*, by:

Maxwell's electromagnetic field equations:

$$\nabla\cdot\mathbf{H}=0,\quad \nabla\cdot\mathbf{E}=\mathbf{0}, \tag{7}$$

$$\nabla\wedge\mathbf{H}=\mathbf{J},\quad \mathbf{J}=\sigma\{\mathbf{E}+\boldsymbol{\mu}_{nf}(\mathbf{V}\wedge\mathbf{H})\}, \tag{8}$$

$$\nabla\wedge\mathbf{E}=-\boldsymbol{\mu}_{nf}\frac{\partial\mathbf{H}}{\partial\mathbf{t}}\cdot \tag{9}$$

D'Alembert mass conservation (continuity) equation:

$$\nabla\cdot\mathbf{V}=\mathbf{0}\cdot \tag{10}$$

Momentum conservation equations:

$$\rho_{nf}\left(\frac{\partial\mathbf{V}}{\partial t}+\mathbf{V}\cdot\nabla\mathbf{V}\right)=-\nabla p+\mu_{nf}\,\mathrm{div}\,\mathbf{V}-\nabla\left(\frac{1}{2}\mu_{nf}\left(H^+\right)^2\right)-\mu_{nf}\left(H^+.\nabla\right)H\cdot \tag{11}$$

Energy (heat) Conservation equation:

$$(\rho c)_f\left(\frac{\partial\mathbf{T}}{\partial t}+\mathbf{V}\cdot\nabla\mathbf{T}\right)=k_{nf}\nabla T+\Phi\cdot \tag{12}$$

Combining Eqs$\cdot$ (2) to (4) we obtain the magnetic induction equation as follows

$$\frac{\partial\mathbf{H}^+}{\partial t}=\nabla\wedge\left(\mathbf{V}\wedge\mathbf{H}^+\right)+\frac{\mu_{nf}}{\mu_f}\frac{1}{\xi}\nabla^2\mathbf{H}^+, \tag{13}$$

where $\zeta=\frac{1}{\sigma\mu_f}$ is the magnetic diffusivity of the nanofluid, ρ_{nf} is the effective density of

the incompressible nanofluid, $(\rho c)_{nf}$ is the heat capacity of the nanofluid, $(\rho c)_p$ is effective heat capacity of the nano particle material, k_{nf} defines effective thermal conductivity, σ is electrical conductivity of magnetic nanofluid, g denotes gravitational acceleration, μ_{nf} is the effective viscosity of the nanofluid, d/dt gives the material time derivative, P is the pressure and Φ is viscous dissipation . The frame of reference may be transformed from a wave to a static one via the subsequent associations (rendering the moving boundary value problem into a static boundary value problem):

$$\bar{x} = \bar{X} - c\bar{t},\ \bar{y} = \bar{Y},\ \bar{u} = \bar{U} - c,\ \bar{v} = \bar{V}.a\,. \tag{14}$$

To further facilitate the analysis, it is judicious to introduce a series of dimensionless parameters, which are defined as follows:

$$\left.\begin{aligned}
&\bar{x} = \frac{x}{\lambda},\ \bar{y} = \frac{y}{a},\ \bar{u} = \frac{u}{c},\ \bar{v} = \frac{v}{c\delta},\ \delta = \frac{a}{\lambda},\ \varepsilon = \frac{b}{a},\\
&\bar{p} = \frac{a^2 p}{\mu_f c\lambda},\ \bar{t} = \frac{ct}{\lambda},\ h = \frac{\bar{h}}{a}, \mathrm{Re} = \frac{ca}{\nu},\ \bar{\Psi} = \frac{\Psi}{ca},\ \theta = \frac{\bar{T} - \bar{T}_0}{\bar{T}_0},\\
&\bar{\Phi} = \frac{\Phi}{H_0 a},\ \overline{\Psi} = \frac{\Psi}{ca},\ R_m = \sigma\boldsymbol{\mu}_f ac,\quad S_1 = \frac{H_0}{c}\sqrt{\frac{\mu_f}{\rho}},\\
&M = \sqrt{\frac{\sigma}{\mu_f}} H_o a\,,
\end{aligned}\right\} \tag{15}$$

where R_m is the magnetic Reynolds number, Re is the ordinary Reynolds number, S_1 is the Størmer number (a dimensionless group introduced originally in magnetospheric physics [48] and of particular relevance in magnetohydrodynamic wave flows), Q is flow rate, θ is dimensionless temperature, ψ is stream function, Br is Brinkman (viscous dissipation) number, E is electric field strength parameter ($= -\frac{E_0}{cH_o\mu_f}$) and M is the Hartmann (magnetic body force) number. Note $M^2 = ReS_1^2 R_m$ and M^2 does not arise explicitly subsequently. All other parameters are normalized versions of the original parameter. After using the above non-dimensional parameters and transformations in Eqs. (6) to (8) employing the assumptions of long wavelength $(\delta \to 0)$, the emerging dimensionless governing equations $(\text{without using bars})$ for magnetohydrodynamic nanofluid flow in the wave frame take the final and much-simplified form:

$$\frac{\partial u}{\partial x}+\frac{\partial v}{\partial y}=0, \tag{16}$$

$$\frac{\partial p}{\partial y}=0, \tag{17}$$

$$\Phi_{yy}=R_m\left(E-\frac{\partial \Psi}{\partial y}\right), \tag{18}$$

$$\frac{k_{nf}}{k_f}\frac{\partial^2\theta}{\partial y^2}+\frac{B_r}{(1-\varphi)^{2.5}}\left(\frac{\partial^2\Psi}{\partial y^2}\right)^2=0 \tag{19}$$

$$\frac{\partial p}{\partial x}=\frac{1}{(1-\varphi)^{2.5}}\frac{\partial^3\Psi}{\partial y^3}+\mathrm{Re}\,S_1^2R_m\left(E-\frac{\partial \Psi}{\partial y}\right), \tag{20}$$

Differentiating Eq.(20) with respect to y ,we get:

$$\frac{1}{(1-\varphi)^{2.5}}\frac{\partial^4\Psi}{\partial y^4}+\mathrm{Re}\,S_1^2R_m\left(-\frac{\partial^2\Psi}{\partial y^2}\right)=0, \tag{21}$$

The following non-dimensional boundary conditions are imposed:

$$\Psi=0,\ \ \frac{\partial^2\Psi}{\partial y^2}=0,\ \text{at}\ \ y=0, \tag{22}$$

$$\Psi=F,\ \ \frac{\partial\Psi}{\partial y}=-1-\frac{2\pi\varepsilon\alpha\beta\cos(2\pi x)}{1-2\pi\varepsilon\alpha\beta\cos(2\pi x)},\ \text{at}\ \ y=h=1+\varepsilon\cos(2\pi x), \tag{23}$$

$$\frac{\partial\theta}{\partial y}=0\ \ \text{at}\ y=0,\quad \theta=0\ \ \text{at}\ y=h, \tag{24}$$

$$\frac{\partial\Phi}{\partial y}=0\ \ \text{at}\ y=0,\quad \Phi=0\ \ \text{at}\ y=h. \tag{25}$$

The thermo-physical properties for copper-water nanofluids are listed in **Table-1**.

Table.1. Thermal properties of base fluid (water) and copper nanoparticles.

Physical Properties	Fluid Phase (Water)	Cu
c_p*(J/kgK)*	4179	385
ρ *(kg/m^3)*	997.1	8933
k(W/mk)	0.613	400

The effective density (ρ_{nf}), effective viscosity (μ_{nf}), specific heat of nanofluid ($(c_p)_{nf}$), thermal diffusivity of nanofluid (α_{nf}) and effective thermal conductivity of nanofluid (k_{nf}) are defined respectively as:

$$\left.\begin{aligned}
&\rho_{nf}=(1-\varphi)\rho_f+\varphi\rho_s,\ \mu_{nf}=\frac{\mu_f}{(1-\varphi)^{2.5}},\\
&\left(\rho c_p\right)_{nf}=(1-\varphi)\left(\rho c_p\right)_f+\varphi\left(\rho c_p\right)_s,\ \alpha_{nf}=\frac{k_{nf}}{\left(\rho c_p\right)_{nf}},\\
&k_{nf}=k_f\left(\frac{k_s+2k_f-2\varphi\left(k_f-k_s\right)}{k_s+2k_f+2\varphi\left(k_f-k_s\right)}\right).
\end{aligned}\right\} \tag{26}$$

4. ANALYTICAL SOLUTIONS

Solving Eq.(21) with boundary conditions (22 & 23), the stream function is obtained as:

$$\Psi(x,y)=\frac{A\left(\cosh\left(\frac{\sqrt{\mathrm{R}_1}\sqrt{\mathrm{R}_\mathrm{m}}S_1y}{\sqrt{A}}\right)-\sinh\left(\frac{\sqrt{\mathrm{R}_1}\sqrt{\mathrm{R}_\mathrm{m}}S_1y}{\sqrt{A}}\right)\right)\left(\mathrm{D}_1\sinh\left(\frac{2\sqrt{\mathrm{R}_1}\sqrt{\mathrm{R}_\mathrm{m}}S_1y}{\sqrt{A}}\right)+\mathrm{D}_1\cosh\left(\frac{2\sqrt{\mathrm{R}_1}\sqrt{\mathrm{R}_\mathrm{m}}S_1y}{\sqrt{A}}\right)+\mathrm{D}_2\right)}{\mathrm{R}_1\mathrm{R}_\mathrm{m}S_1^2}$$
$$+\mathrm{D}_3+\mathrm{D}_4y. \tag{27}$$

Using Eq.(27) in Eq.(20), yields the pressure gradient as:

$$\frac{\partial P}{\partial x}=\frac{\sqrt{\mathrm{R}_1}\sqrt{\mathrm{R}_\mathrm{m}}S_1(F+hL+h)\left(\sinh\left(\frac{2h\sqrt{\mathrm{R}_1}\sqrt{\mathrm{R}_\mathrm{m}}S_1}{\sqrt{A}}\right)+\cosh\left(\frac{2h\sqrt{\mathrm{R}_1}\sqrt{\mathrm{R}_\mathrm{m}}S_1}{\sqrt{A}}\right)+1\right)}{\mathrm{D}_5}-L-1. \tag{28}$$

The dimensionless pressure rise, ΔP , is defined as:

$$\Delta P=\int_0^1\left(\frac{\partial P}{\partial x}\right)dx\cdot \tag{29}$$

Using Eq.(27) in Eq.(18) with the boundary conditions (25), the *induced magnetic field* takes the form

$$\Phi(x,y)=\mathrm{D}_{10}\sinh\left(\frac{\sqrt{\mathrm{R}_1}\sqrt{\mathrm{R}_\mathrm{m}}S_1y}{\sqrt{A}}\right)+\mathrm{D}_9\cosh\left(\frac{\sqrt{\mathrm{R}_1}\sqrt{\mathrm{R}_\mathrm{m}}S_1y}{\sqrt{A}}\right)-\frac{1}{2}\mathrm{D}_4\mathrm{R}_\mathrm{m}y^2+\mathrm{D}_7+\mathrm{D}_8y+\frac{1}{2}\mathrm{E}_1\mathrm{R}_\mathrm{m}y^2 \tag{30}$$

Using Eq.(27) in Eq.(19) with boundary conditions (24), the *temperature field* is found to be:

$$\theta(x,y)=-\frac{A\mathrm{B}_1\mathrm{D}_1\mathrm{D}_2y^2}{\mathrm{Kf}}+\mathrm{D}_{16}\cosh\left(\frac{2\sqrt{\mathrm{R}_1}\sqrt{\mathrm{R}_\mathrm{m}}S_1y}{\sqrt{A}}\right)+\mathrm{D}_{17}\mathrm{Sinh}\left(\frac{2\sqrt{\mathrm{R}_1}\sqrt{\mathrm{R}_\mathrm{m}}S_1y}{\sqrt{A}}\right)+\mathrm{D}_{14}+\mathrm{D}_{15}\mathrm{y} \tag{31}$$

where the following definitions apply:

$$D_1 = -\frac{\mathrm{R_1 R_m} S_1^2 (F + hL + h)\left(\sinh\left(\frac{h\sqrt{\mathrm{R_1}}\sqrt{\mathrm{R_m}} S_1}{\sqrt{A}}\right) + \cosh\left(\frac{h\sqrt{\mathrm{R_1}}\sqrt{\mathrm{R_m}} S_1}{\sqrt{A}}\right)\right)}{\sqrt{A}\mathrm{D_5}}, \quad (32)$$

$$D_2 = \frac{\mathrm{R_1 R_m} S_1^2 (F + hL + h)\left(\sinh\left(\frac{h\sqrt{\mathrm{R_1}}\sqrt{\mathrm{R_m}} S_1}{\sqrt{A}}\right) + \cosh\left(\frac{h\sqrt{\mathrm{R_1}}\sqrt{\mathrm{R_m}} S_1}{\sqrt{A}}\right)\right)}{\sqrt{A}\mathrm{D_5}}, \quad (33a, b)$$

$$D_3 = 0,$$

$$D_4 = \frac{\sqrt{\mathrm{R_1}}\sqrt{\mathrm{R_m}} S_1 (F + hL + h)\left(\sinh\left(\frac{2h\sqrt{\mathrm{R_1}}\sqrt{\mathrm{R_m}} S_1}{\sqrt{A}}\right) + \cosh\left(\frac{2h\sqrt{\mathrm{R_1}}\sqrt{\mathrm{R_m}} S_1}{\sqrt{A}}\right) + 1\right)}{\mathrm{D_5}} - L - 1, \quad (34)$$

$$\mathrm{D_5} = h\sqrt{\mathrm{R_1}}\sqrt{\mathrm{R_m}} S_1 \sinh\left(\frac{2h\sqrt{\mathrm{R_1}}\sqrt{\mathrm{R_m}} S_1}{\sqrt{A}}\right) - \sqrt{A}\sinh\left(\frac{2h\sqrt{\mathrm{R_1}}\sqrt{\mathrm{R_m}} S_1}{\sqrt{A}}\right) + \mathrm{D_6}, \quad (35)$$

$$\mathrm{D_6} = h\sqrt{\mathrm{R_1}}\sqrt{\mathrm{R_m}} S_1 \cosh\left(\frac{2h\sqrt{\mathrm{R_1}}\sqrt{\mathrm{R_m}} S_1}{\sqrt{A}}\right) - \sqrt{A}\cosh\left(\frac{2h\sqrt{\mathrm{R_1}}\sqrt{\mathrm{R_m}} S_1}{\sqrt{A}}\right) + \sqrt{A} + h\sqrt{\mathrm{R_1}}\sqrt{\mathrm{R_m}} S_1, \quad (36)$$

$$\mathrm{D_7} = \frac{2A^{3/2}\mathrm{D_{11}} - \mathrm{h_1 h_2 R_1^{3/2} R_m^{3/2}} S_1 (\mathrm{D_4} - \mathrm{E_1})(\mathrm{h_1} - \mathrm{h_2})}{2\mathrm{R_1^{3/2}}\sqrt{\mathrm{R_m}} S_1^3 (\mathrm{h_1} - \mathrm{h_2})}, \quad (37)$$

$$\mathrm{D_8} = \frac{2A^{3/2}\mathrm{D_4} + \mathrm{R_1^{3/2} R_m^{3/2}} S_1^3 (\mathrm{D_4} - \mathrm{E_1})(\mathrm{h_1} - \mathrm{h_2})(\mathrm{h_1} + \mathrm{h_2})}{2\mathrm{R_1^{3/2}}\sqrt{\mathrm{R_m}} S_1^3 (\mathrm{h_1} - \mathrm{h_2})}, \quad (38)$$

$$\mathrm{D_9} = \frac{A^{3/2}\mathrm{D_2}}{\mathrm{R_1^{3/2}}\sqrt{\mathrm{R_m}} S_1^3} - \frac{A^{3/2}\mathrm{D_1}}{\mathrm{R_1^{3/2}}\sqrt{\mathrm{R_m}} S_1^3}, \quad (39)$$

$$\mathrm{D_{10}} = -\frac{A^{3/2}\mathrm{D_1}}{\mathrm{R_1^{3/2}}\sqrt{\mathrm{R_m}} S_1^3} - \frac{A^{3/2}\mathrm{D_2}}{\mathrm{R1^{3/2}}\sqrt{\mathrm{R_m}} S_1^3}, \quad (40)$$

$$D_{11} = D_{12} + D_{13}, \quad (41)$$

$$\mathrm{D_{12}} = (\mathrm{D_2 h_2} - \mathrm{D_1 h_2})\cosh\left(\frac{\mathrm{h_1}\sqrt{\mathrm{R_1}}\sqrt{\mathrm{R_m}} S_1}{\sqrt{A}}\right) + (\mathrm{D_1 h_1} - \mathrm{D_2 h_1})\cosh\left(\frac{\mathrm{h_2}\sqrt{\mathrm{R_1}}\sqrt{\mathrm{R_m}} S_1}{\sqrt{A}}\right), \quad (42)$$

$$\mathrm{D_{13}} = (-\mathrm{D_1 h_2} - \mathrm{D_2 h_2})\sinh\left(\frac{\mathrm{h_1}\sqrt{\mathrm{R_1}}\sqrt{\mathrm{R_m}} S_1}{\sqrt{A}}\right) + (\mathrm{D_1 h_1} + \mathrm{D_2 h_1})\sinh\left(\frac{\mathrm{h_2}\sqrt{\mathrm{R_1}}\sqrt{\mathrm{R_m}} S_1}{\sqrt{A}}\right), \quad (43)$$

$$\mathrm{D_{14}} = \frac{A\mathrm{B_1}\left(2\sqrt{A}h\sqrt{\mathrm{R_1}}\sqrt{\mathrm{R_m}} S_1 \left(\mathrm{D_2^2} - \mathrm{D_1^2}\right) + 4\mathrm{D_1 D_2} h_1^2 \mathrm{R_1 R_m} S_1^2 + \mathrm{D_{20}}\right.}{4\mathrm{K_f R_1 R_m} S_1^2}, \quad (44)$$

$$D_{15} = \frac{A^{3/2} B_1 (D_1 - D_2)(D_1 + D_2)}{2K_f \sqrt{R_1}\sqrt{R_m} S_1}, \tag{45}$$

$$D_{16} = -\frac{A^2 B_1 D_1^2}{4K_f R_1 R_m S_1^2} - \frac{A^2 B_1 D_2^2}{4K_f R_1 R_m S_1^2}, \tag{46}$$

$$D_{17} = \frac{A^2 B_1 D_1^2}{4K_f R_1 R_m S_1^2} - \frac{A^2 B_1 D_2^2}{4K_f R_1 R_m S_1^2}, \tag{47}$$

$$D_{18} = A\left(\cosh\left(\frac{2h_1 \sqrt{R_1}\sqrt{R_m} S_1}{\sqrt{A}} \right) - \sinh\left(\frac{2h \sqrt{R_1}\sqrt{R_m} S_1}{\sqrt{A}} \right) \right), \tag{48}$$

$$D_{19} = D_1^2 \sinh\left(\frac{4h_1 \sqrt{R_1}\sqrt{R_m} S_1}{\sqrt{A}} \right) + D_1^2 \cosh\left(\frac{4h_1 \sqrt{R_1}\sqrt{R_m} S_1}{\sqrt{A}} \right) + D_2^2, \tag{49}$$

$$D_{20} = D_{19} D_{18}. \tag{50}$$

5. RESULTS AND DISCUSSION

Extensive computations have been conducted to determine the influence of magnetic Reynolds number (R_m), Reynolds number (Re), Størmer magnetic induction number (S_1.), hydrodynamic flow rate (Q), Brinkman number (Br), wave amplitude (ϕ) and electric current parameter (E) on the various flow variables. These are depicted in Figs. 2-9.

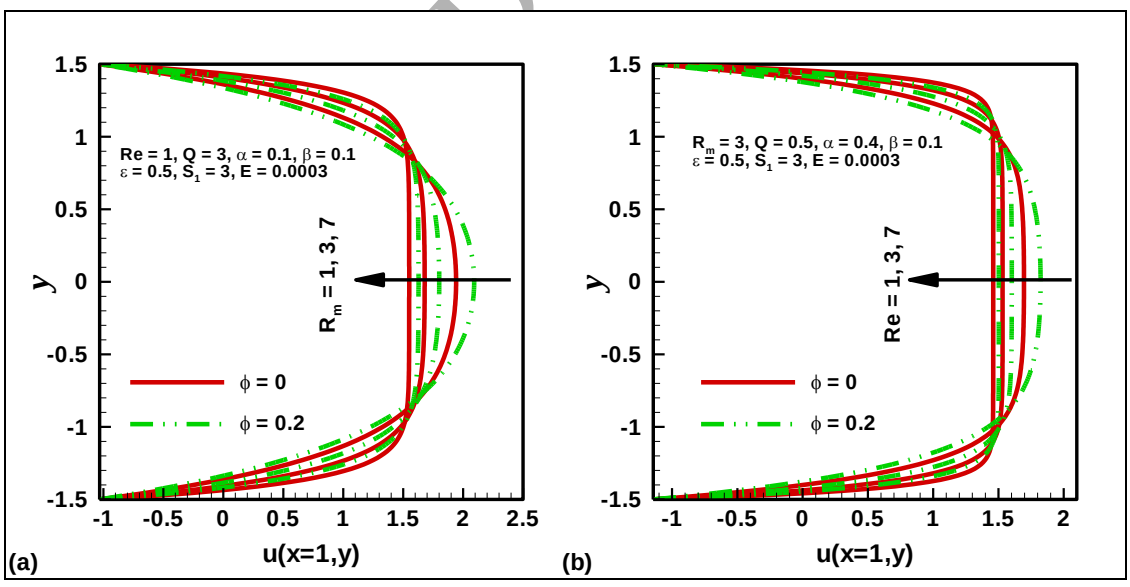

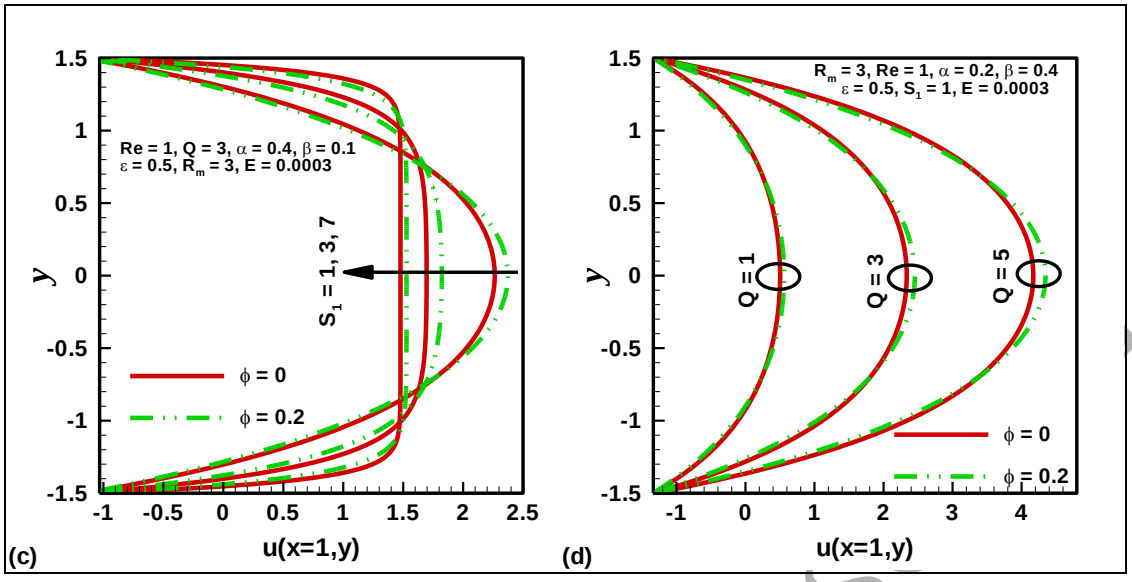

Fig. 2. Velocity profiles for different values of (a) Magnetic Reynolds number (R_m), (b) Reynolds number (Re), (c) Størmer number (S_1), (d) Flow rate (Q).

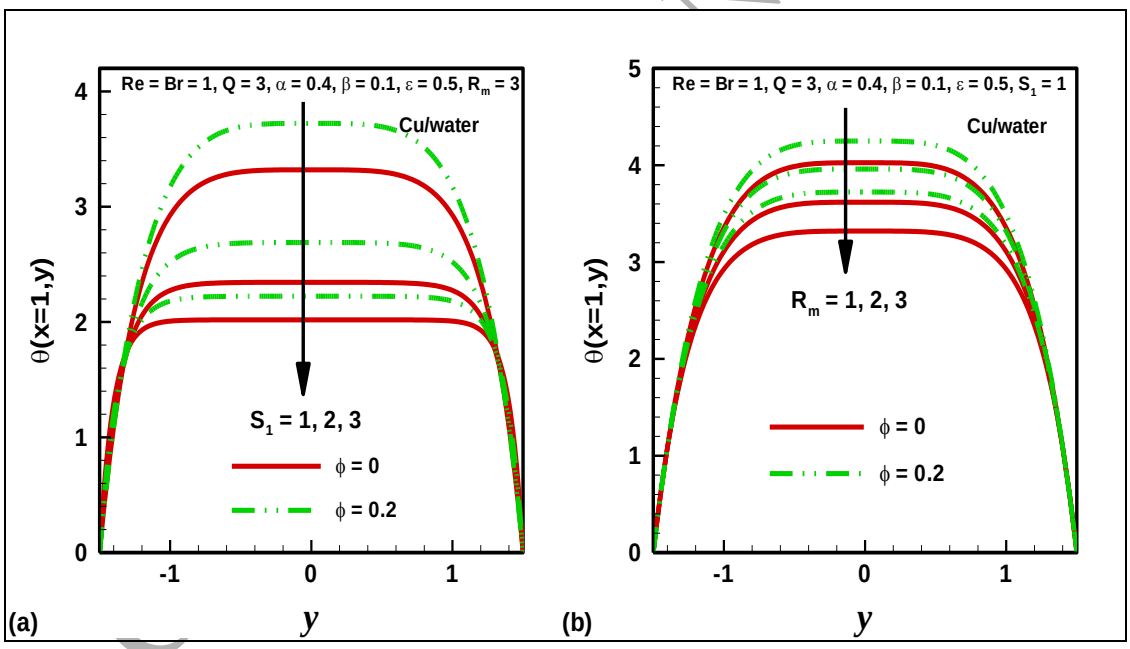

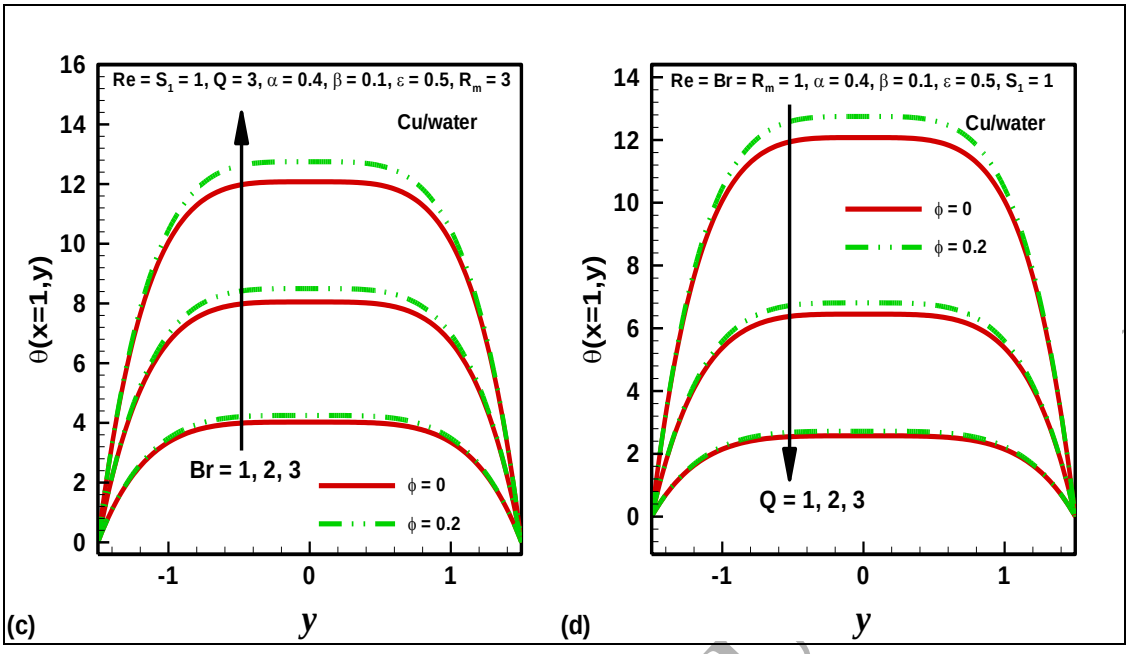

Fig. 3. Temperature profiles for different values of (a) Størmer number (S_1), (b) Magnetic Reynolds number (R_m), (c) Brinkman number (Br), (d) Flow rate (Q).

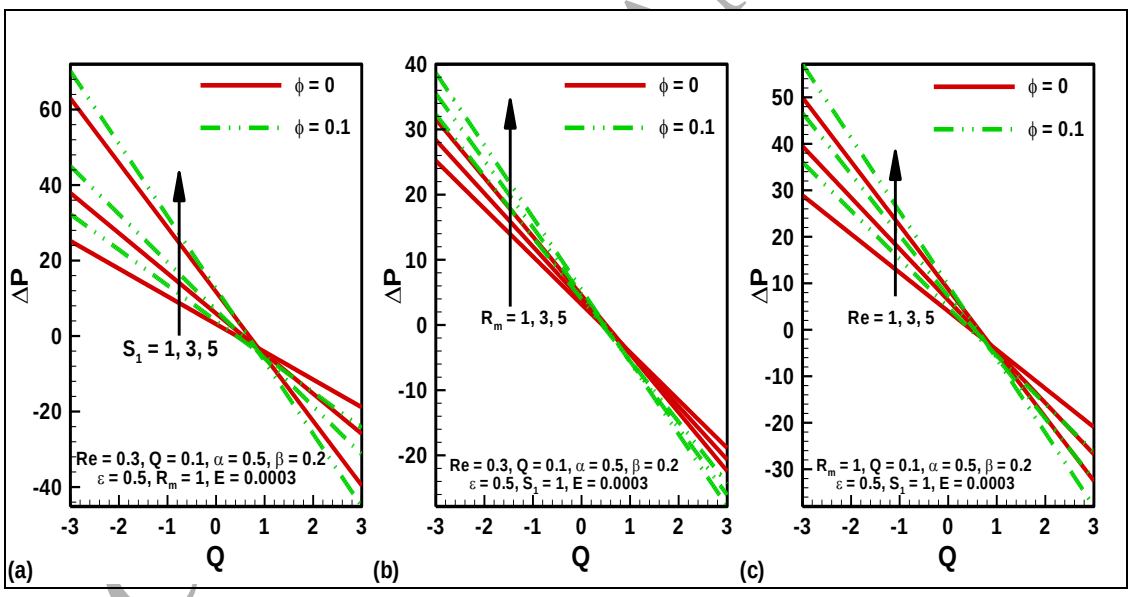

Fig.4. Pressure rise for different values of (a) Størmer number (S_1), (b) Magnetic Reynolds number (R_m), (c) Reynolds number (Re).

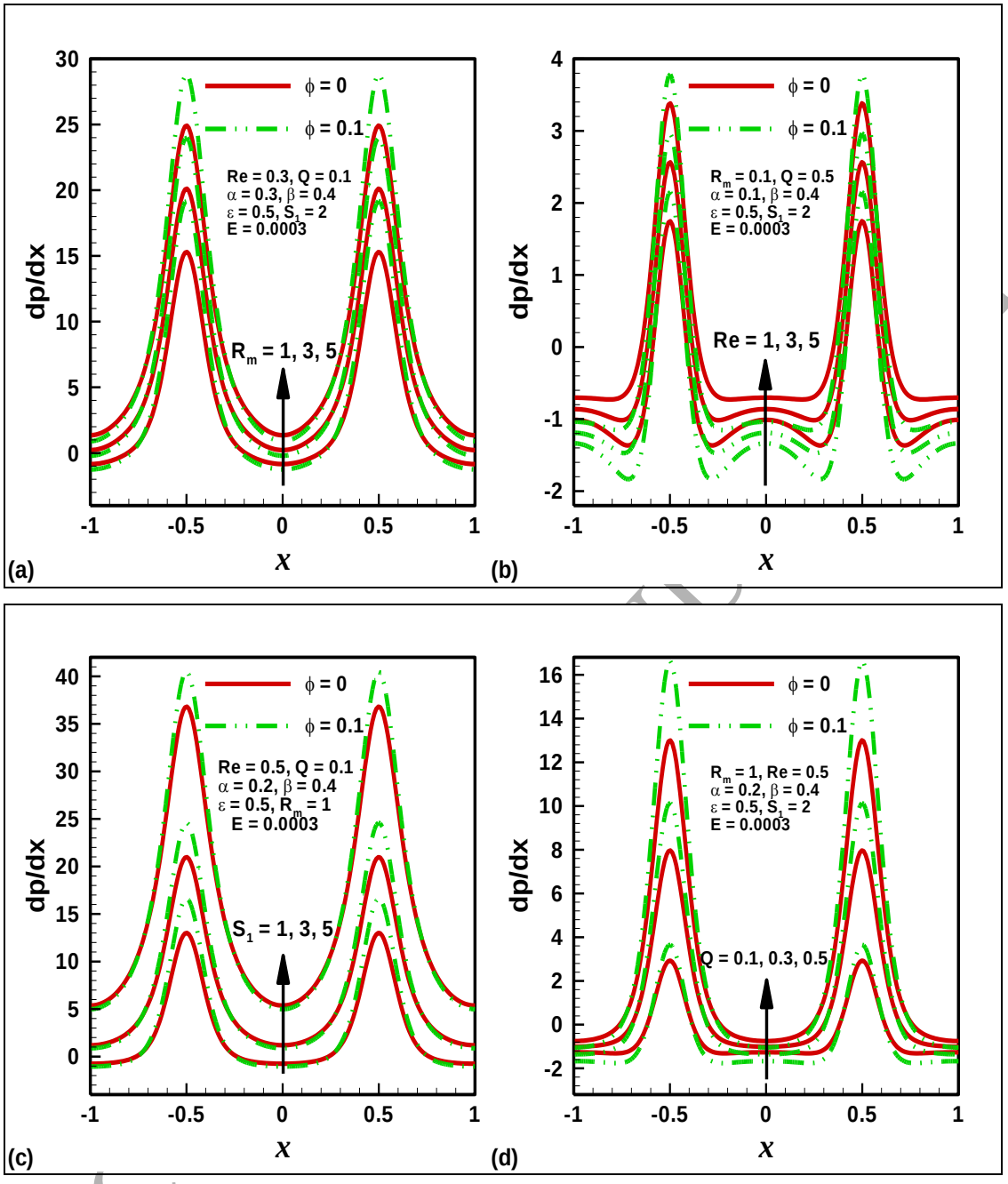

Fig. 5. Pressure gradient for different values of (a) Magnetic Reynolds number (R_m), (b) Reynolds number (Re), (c) Størmer number (S_1), (d) Flow rate (Q).

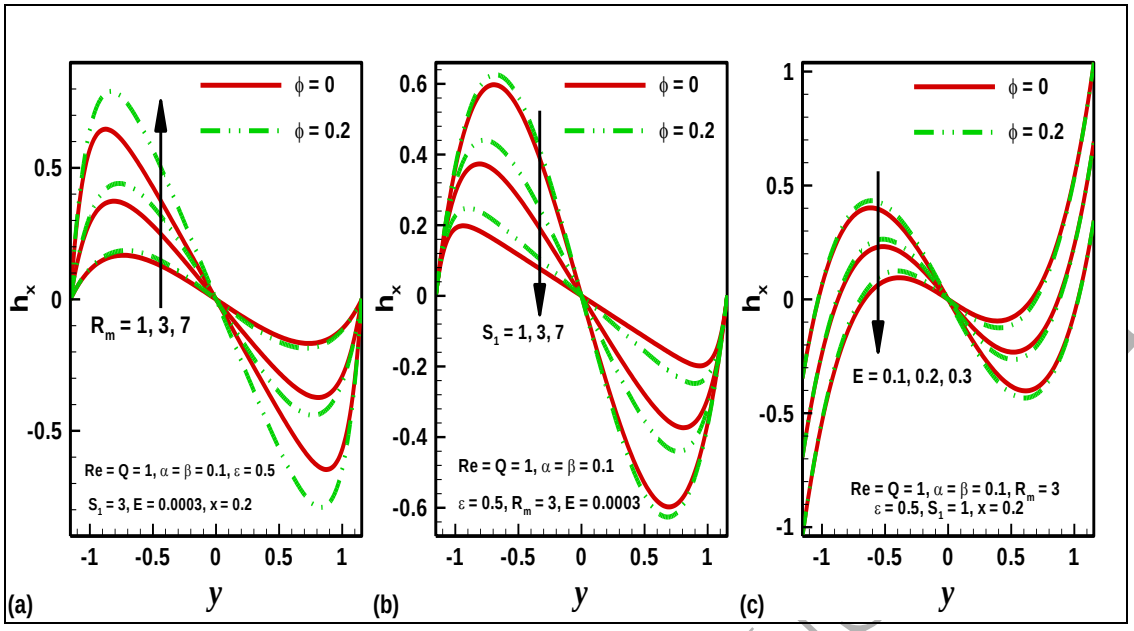

Fig.6. Variation of induced magnetic field for different values of (a) Magnetic Reynolds number (R_m), (b) Størmer number (S_1), (c) Electric current (E) .

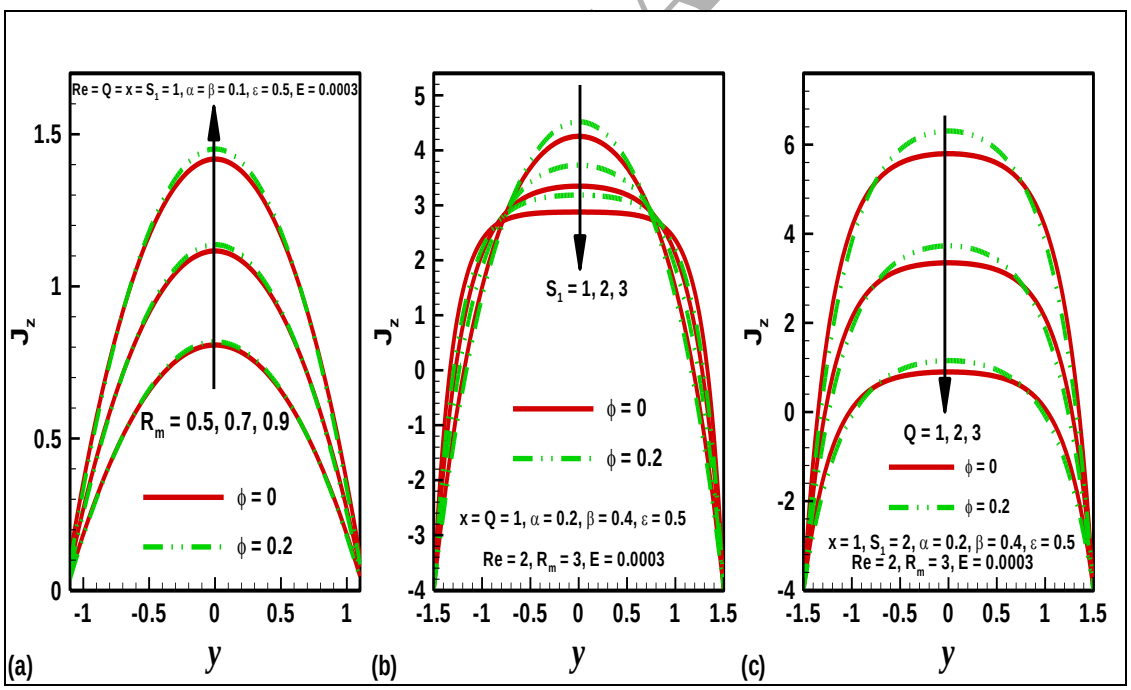

Fig.7. Variation of current density for different values of (a) Magnetic Reynolds number (R_m), (b) Størmer number (S_1), (c) Flow rate (Q).

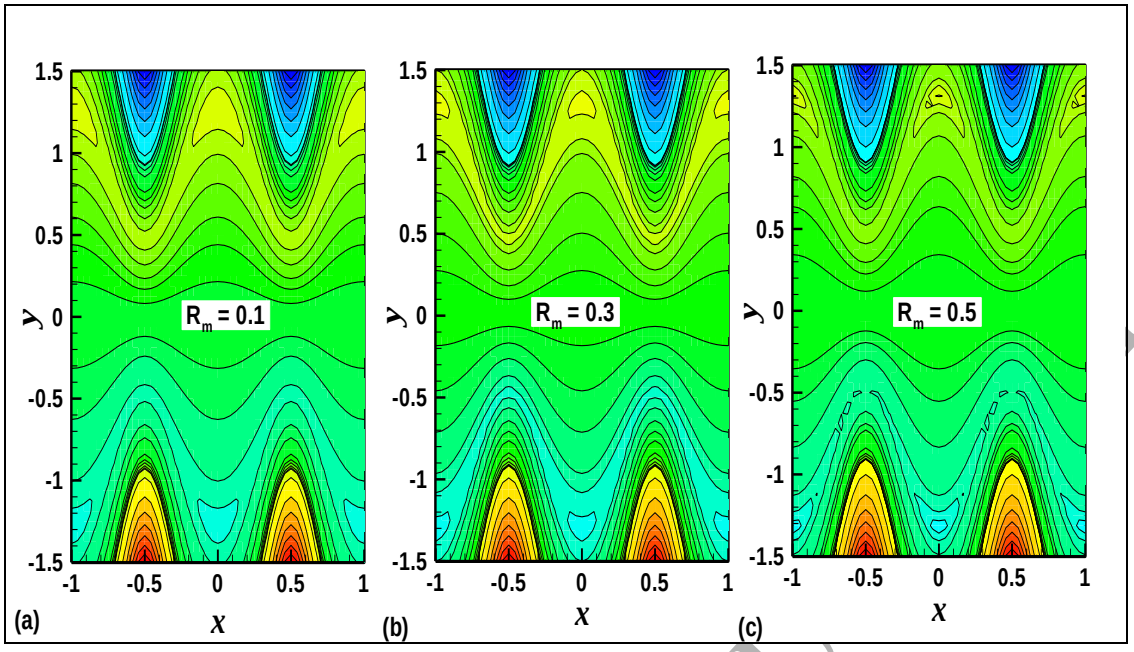

Fig.8. Streamlines for different values of magnetic Reynolds number (R_m) with S_1 = 0.4, *Re =0.4, α = 0.4, β = 0.3, Q = 0.6, x = 1*.

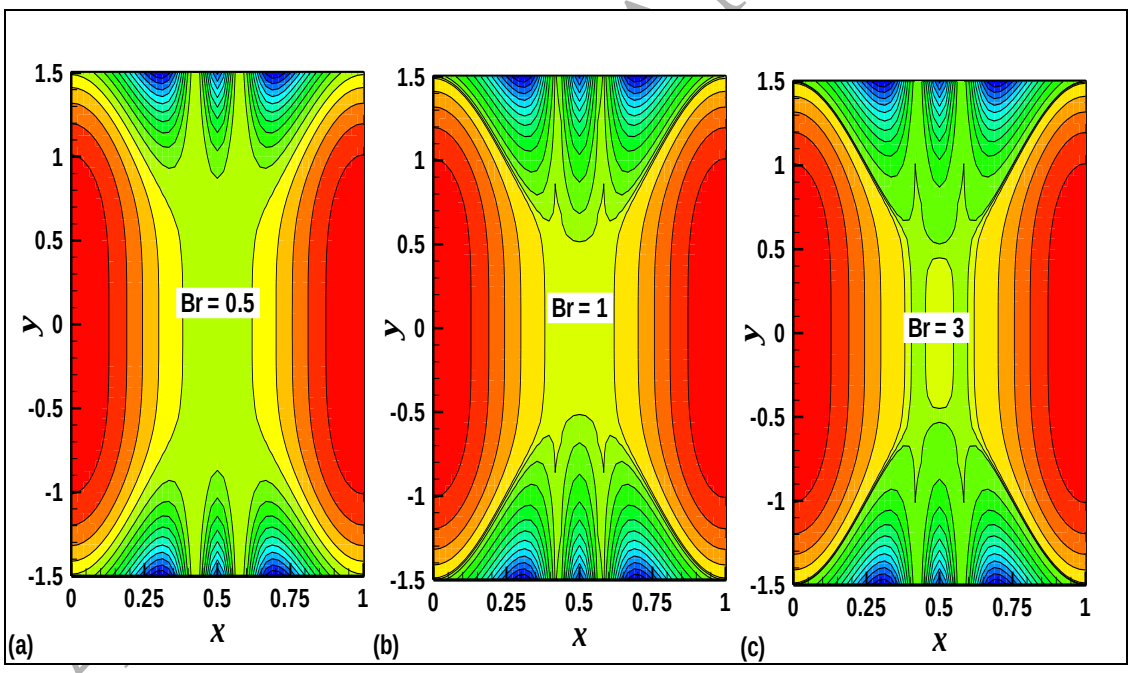

Fig.9. Isotherms for different values of Brinkman number (*Br*) other parameters are S_1 = *0.4, Re =0.4, α = 0.4, β = 0.3, Q = 0.6, x = 1,* R_m = *2*.

Figs.2a-d depict the evolution of axial velocity, u, with respectively, (a) magnetic Reynolds number (R_m), (b) Reynolds number (Re), (c) Størmer number (S_1), (d) flow rate (Q). In these figures the other parameters are fixed, namely α and β (parameters which relate to the geometric wave definitions in Eq.(23) wherein α quantifies eccentricity of the cilia elliptical motion) and ε (cilia length parameter). However two cases of ϕ (nano-particle solid volume fraction) variation are incorporated (red solid line for $\phi = 0$ *i.e. pure fluid without nano-particles* and green dashed line for $\phi = 0.2$ *which corresponds to the copper nanofluid case*). The variation in cilia length in particular is not studied as this has been examined in quite some detail in earlier studies e.g. Akbar *et al*. [15, 16]. It is however worthy of elaborating again that cilia spacing and length influences the viscous resistance per cilium and thereby the axial flow. The latter is assisted with greater cilia length and this will assist in pressure rise in the lower channel half space. The introduction of extra energy to the flow at the lower wall however must be compensated for by an extraction at the upper wall, and these features are also related to synchronicity of beating cilia. The special case of $\varepsilon = 0$ implies vanishing cilia and absence of a metchronal wave in this scenario the flow is a purely peristaltic mechanism due to flexibility of the walls. Only for $\varepsilon > 0$ is the cilia effect invoked and this indeed is the case considered throughout the present analysis ($\varepsilon = 0.5$ in all Figs.2-9). Fig.2a reveals that with increasing magnetic Reynolds number, there is a depletion in velocity magnitudes across the channel width. At y = -1.5 (lower channel plate) and again at y = 0.5 (upper channel plate) velocity vanishes in consistency with the no slip conditions imposed. The strongly parabolic velocity distributions in the core region of the flow which are observed at lower R_m values are flattened significantly with increasing R_m values. Magnetic Reynolds number is the ratio of the fluid flux to the magnetic diffusivity. It characterizes the diffusion of magnetic field along streamlines and is analogous to the classical Reynolds number in viscous hydrodynamics, the latter controlling the vorticity diffusion along the streamlines. As such the influence of the fluid flow on the magnetic field is embodied in magnetic Reynolds number. Low R_m values ($<<1$) the magnetic field will not be markedly distorted by the flow. However, as in the present study, for R_m values (≥ 1), the hydrodynamics influences considerably the induced magnetic field distribution which is tangibly distorted. However there is also a reciprocating influence on the flow field. Greater

R_m values lead to a flow deceleration i.e. momentum diffusion is inhibited. However this effect is restricted only to the core (plug) flow region and does not apply near the vicinity of the channel walls. At the latter the destruction in momentum in the core flow is compensated for with a boost in momentum at the external periphery of the flow field (near both channel plates) resulting in a flow acceleration here with higher magnetic Reynolds numbers. With presence of copper nano-particles (i.e. for $\phi = 0.2$) the velocities are generally significantly greater in the core region compared with pure fluid (i.e. for $\phi = 0$). This would imply that flow acceleration is achieved with nano-particle presence. However in the near-plate zones, the opposite effect is observed with flow deceleration induced with nano-particles. Fig.2b shows that increasing ordinary Reynolds number (*Re*) there is in fact a deceleration in the core-flow (a strong plateau effect is induced in velocity profiles). However at the near-wall zones, the greater inertial forces corresponding to higher Reynolds number (and reduced viscous forces) manifest in a noticeable acceleration in the axial flow. As noted earlier, greater velocities are achieved with nano-particle presence in the core flow whereas lower velocities are computed in the zones near the plates. An increase in Størmer number (S_1), as illustrated in Fig.2c, generally depresses core region velocity magnitudes. Whereas the Hartmann number (*M*) is conventionally employed for static magnetic field phenomena to simulate Lorentzian magnetic drag effects, the Størmer number (S_1), is more appropriate for flow regimes with moving boundaries and wave effects. The definition of Størmer number i.e. $S_1 = \frac{H_o}{c}\sqrt{\frac{\mu_f}{\rho}}$ scales as the *inverse of wave speed of the metachronal wave* (*c*). Hartmann number is however defined as $M = \sqrt{\frac{\sigma_1}{\mu_f}} H_o a$ and therefore while it scales with nanofluid electrical conductivity, applied magnetic field, base fluid viscosity and channel half-width, it *does not scale* with metachronal wave speed (*c*). Therefore via the definition given earlier, viz, $M^2 = ReS_1^2 R_m$, here we opt to examine the individual effects of the component dimensionless numbers, $ReS_1^2 R_m$, rather than the global effect via the Hartmann number. We further note that axial induced magnetic field component, h_x, and current density component, J_z, studied in later graphs, can also be explicitly defined with the relations given in Eq.(15). Effectively a flow deceleration corresponds to greater Størmer number (S_1) in the core zone (bulk flow) of the channel, whereas the converse effect is generated near the plates. The

greater applied magnetic field corresponding to larger Størmer number contributes to the impedance effect in the core flow (retardation). A re-distribution of momentum in the regime occurs. Momentum lost in the core region must be compensated elsewhere in accordance with momentum conservation, and this leads to the acceleration of the axial flow near the plates at higher Størmer numbers. In the core zone nano-particle presence results in greater velocities with the contrary apparent again near the plates. With increasing flow rate (Fig.4d) there is a significant boost in the axial velocity across the entire channel. The profiles are always parabolic, unlike the other distributions in Figs.2a-c (which are plateau-like in the core flow zone). There is a slight acceleration in the flow for the nanofluid case, compared with the pure fluid case.

Figs.3a-d illustrate the temperature distribution, θ, with variation in (a) Størmer number (S_1), (b) magnetic Reynolds number (R_m), (c) Brinkman number (Br) and finally (d) flow rate (Q). Again we consider both nanofluid and pure fluid cases via the variation in nano-particle solid fraction (ϕ). An increase in Størmer number (S_1) as seen in Fig. 3a, generates a strong decrease in temperature i.e. cools the channel nanofluid flow regime in the core zone. However a slight increase is observed near both plates. With magnetic induction present and with larger magnetic Reynolds numbers, the effect of heating with greater magnetic field (traditionally associated with the dissipation in supplementary work done to drag fluid against the action of magnetic field, as thermal energy i.e. heat), is reversed, and a cooling effect observed. Nanofluid (copper-water) however attains significantly greater temperatures than the pure fluid (zero solid volume fraction). The depressive nature of magnetic field, in the presence of magnetic induction, is further confirmed with Fig.3b, where we find that greater magnetic Reynolds number markedly lowers the temperature across the channel. Again nanofluids supersede pure fluids in achieving substantially greater temperatures, despite the presence of magnetic induction effects. Fig.3c shows that an elevation in the viscous heating parameter i.e. Brinkman number (Br), significantly raises temperature in the regime, and again greater temperatures correspond to the copper-water nanofluid case (ϕ=0.2) compared with the pure fluid case (ϕ=0). Brinkman number is a quantification of the relative influence of viscous dissipation to the conductive heat transfer in thermofluid mechanics. For $Br = 1$ both mechanisms contribute equally. When $Br > 1$, viscous dissipation dominates thermal conduction, as elaborated in Bejan [43]. An increase in Brinkman number

effectively energizes the fluid and boosts thermal energy magnitudes associated with the dissipation of kinetic energy in the nanofluid, and this results in a clear enhancement in temperatures. These results agree with many other studies on dissipative flows e.g. Gorla *et al*. [44]. With increasing flow rate, *Q*, however temperatures are strongly reduced. The greater momentum flux associated with higher flow rates implies that momentum diffusion greatly exceeds thermal diffusion in the channel flow. This serves to accelerate the flow but to simultaneously cool it and thereby decrease temperatures. We further note that despite the negative influence of flow rate on temperatures, the presence of nano-particles is consistently to elevate temperatures relative to pure fluids. The combined effect of viscous heating ($Br = 3$) and deployment of copper-water nanofluids (ϕ=0.2) is overall found to achieve the highest thermal performance in the flow regime studied.

Figs. 4a-c present the profiles for pressure rise (ΔP) with variation in a) Størmer number (S_1), b) magnetic Reynolds number (R_m) and (c) Reynolds number (Re). Increasing Størmer number (S_1) as plotted in Fig.4a, generates a strong elevation in pressure rise for negative flow rates (flow in the reverse axial direction) whereas it results in a significant reduction in pressure rise generally for positive flow rates. The former where $\Delta P > 0$ corresponds to the so-called pumping region, and the latter wherein $\Delta P < 0$ is associated with the co-pumping region. In the former region, nanofluids are found to enhance pressure rise whereas in the latter region they are found to depress pressure rise. There is therefore an intricate interaction between the nature of pumping in the regime and the influence of nano-particles in the conducting nanofluid. In all cases, the ΔP profiles are observed to follow a linear with flow rate (Q). Fig.4b shows that increasing magnetic Reynolds number is observed, similarly to Stormer number, to enhance pressure rise for negative flow rates and to depress them with positive flow rates. The inverse relationship of ΔP with Q is again observed. Fig.4c demonstrates that with increasing Reynolds number, as with magnetic Reynolds number, the pressure rise is accentuated for negative flow rate and reduced for positive flow rate. Again there is a linear decay in pressure rise with flow rate. In all three plots, the highest pressure rise computed corresponds to the copper nanofluid case at the maximum negative flow rate. Nano-particles are observed to enhance pressure rise only for negative flow rates; the converse is the case for positive flow rates.

Figs.5a-c depict the axial pressure gradient (dP/dx) profiles with axial coordinate for a) magnetic Reynolds number (R_m), (b) Reynolds number (Re), c) Størmer number (S_1) and flow rate (Q), again for both copper nanofluid and pure fluid cases. The periodic nature of the flow due to metchronal wave propagation is evident from the oscillatory distributions. There is a consistent elevation in peak magnitudes of pressure gradient with greater magnetic Reynolds number (R_m), as shown in Fig.5a. Similarly increasing Reynolds number, Re, also elevates the pressure gradient magnitudes. However the magnitudes are significantly greater (an order of magnitude larger) in Fig.5a as compared with Fig.5b. With greater Stormer number, S_1, a large enhancement in pressure gradient values is also witnessed and these are of a similar magnitude to those computed with variation in magnetic Reynolds number in Fig.5a. Considerable elevation in pressure gradient also accompanies a rise in flow rate, as seen in Fig.5b, although the magnitudes are somewhat lower than those corresponding to Figs.5a and c, but markedly greater than those in Fig.5b. Effectively greater pressure gradients are generated in the flow with increase in the magnetohydrodynamic parameters (R_m, S_1) compared with the hydrodynamic parameters (Re, Q). This implies that in practical nano-biomedical devices, a stronger effect can be achieved via magnetic field manipulation compared with inertial effects associated with the pumping flow itself. The presence of nano-particles is found to have a consistently assistive effect on pressure gradient with variation in magnetic Reynolds, Stormer and flow rate numbers (Figs.5a-c); however in Fig.5b, where Reynolds number is varied, the copper nanofluid generally only boosts pressure gradient in the vicinity of the peaks of the periodic profiles whereas it is found to deplete pressure gradient in the trough zones.

Figs.6a-c illustrate the response in axial induced magnetic field (h_x) with spanwise channel coordinate (y), for variation in respectively, (a) magnetic Reynolds number (R_m). (b) Størmer number (S_1) and finally (c) electric current (field strength) parameter (E). In all three graphs, in one half region, the induced magnetic field is in one direction whereas in the other half, it is found to be in the opposite direction. This trend is known to be characteristic of magnetic induction field, as discussed Ghosh *et al.* [33]. Indeed it has earlier also been reported by Mekheimer [38] and Hayat *et al*. [41] although these later studies do not physically interpret the results. Positive magnitudes of induced magnetic field are computed with negative y values (lower channel half space) and negative values of induced magnetic field with positive

y values (upper channel half space). In accordance with non-conducting plate boundaries, magnetic induction is found to vanish at $y = \pm 1$. As magnetic Reynolds number increases (Fig.6a), there is a distinct enhancement in positive magnetic induction (h_x) in the lower channel half space, whereas a strong depression is generated for the upper channel half space. The increase in R_m implies, with fixed fluid viscosity, channel half-width and metachronal wave velocity (i.e. μ_f, a, c), that electrical conductivity of the nanofluid is elevated. This boosts the magnetic induction effect and results in greater h_x magnitudes, whether positive or negative. Although Fig.6b demonstrates a similar pattern to that in Fig.6a, the effect of increasing Stormer number is found to be the opposite to that of increasing magnetic Reynolds number. Larger values of Stormer number significantly depress the axial induced magnetic field component, h_x, in the lower channel half space, whereas they elevate h_x values in the upper channel half space. In both Figs.6a, b, the presence of nano-particles (i.e. copper nanofluid case with $\phi = 0.2$) is found to decrease induced magnetic field, h_x, in the lower channel half-space, but to enhance h_x values in the upper channel half-space. An increase in electrical field strength parameter, E, in Fig.6c evidently depressed significantly the axial induced magnetic field component, h_x, in the lower channel half-space whereas it enhances magnitudes in the upper channel half-space. The profiles also deviate substantially from Figs.6a,b, in that the h_x values are equal and opposite at the two channel plates i.e. h_x=-1 at y = -1 whereas h_x = +1 at y =+1. Although the opposite trends for h_x are computed in the two channel half-spaces, h_x magnitudes do not vanish at the plates with variation in electrical field strength. Evidently therefore the electrical field present, which is at right angles to the applied magnetic field (mutually orthogonal), generates a different response in the induced magnetic field distributions compared with parameters associated with the applied magnetic field, $E = -\frac{E_0}{cH_o\mu_f}$, and scales inversely with applied magnetic field and is directly proportional to electrical field, E_0. Conversely the magnetic and Stormer numbers by definition in Eq.(15) are directly proportional to applied magnetic field, H_o. The main effect of increasing electrical field parameter will be to boost the current density, J_z, an observation. Once again the axial induced magnetic field magnitudes are greater for the copper nanofluid compared with pure fluid in the lower channel half space with the reverse trend observed in the upper channel half-space.

Figs. 7a-c present the current density distributions (J_z) with (a) magnetic Reynolds number (R_m), (b) Størmer number (S_1) and (c) flow rate (Q). The profiles are notably distinct in appearance from the axial induced magnetic field profiles of Figs.6a-c. The current density profiles are all parabolic across the entire channel space, with peak values arising only at the channel centre, the maximum simultaneous distance from either plate. With increasing magnetic Reynolds number, J_z values are weakly increased (Fig.7a), whereas with greater Stormer number (Fig.7b) magnitudes are more strongly depressed. In Fig.7c with increasing flow rate, a very strong reduction is computed in current density magnitudes. In Figs.7b, c both positive and negative values of current density are observed whereas generally only positive values are computed in Fig.7a. In all cases the copper nanofluid ($\phi = 0.2$) achieves greater magnitudes of current density than the pure fluid ($\phi = 0$), demonstrating that nano-particles enhance current density, albeit relatively weakly.

Figs.8a-c depict the hydrodynamic streamlines with different magnetic Reynolds numbers (R_m). These graphs are included to illustrate the trapping phenomenon in which an internally circulating bolus of the fluid is formed by closed streamlines. The trapped bolus is displaced and pushed ahead along the channel in the axial direction with the speed of the metchronal wave. Bolus magnitude is found to be slightly enhanced with greater magnetic Reynolds number, with all other parameters invariant. Progressively greater distortion of streamlines is generated in the central zones of the plots with higher values of electrical conductivity, to which magnetic Reynolds number is directly proportional. This encourages bolus growth rather than mitigating it. This trend is found to be in agreement with for example Hayat *et al*. [41] who also considered magnetic induction effects. where electromagnetic induction and electrical current density effects are neglected. The inclusion of such effects therefore significantly modifies the streamline distributions.

Fig. 9 presents isotherm plots across the channel with variation in the dissipation parameter, Brinkman number (*Br*). As Br is increased a central zone of thermal bolus emerges. The isotherms become less constricted above and below this thermal bolus and this results from the increasingly more intense conversion of kinetic energy in the flow to thermal energy via viscous heating. This will also have an impact on streamline distribution and inevitably there will be an interaction with magnetic induction and electrical current density fields both for copper water nanofluids and pure fluids.

y	u(x,y) Present results ($\phi = 0.00$)	Refs. [16]	Ref. [33]	Ref. [42] in absence of Heat and Mass Transfer
-0.8	-1.0000	-1.0000	-1.0000	-1.0000
-0.6	-0.1008	-0.1006	-0.1008	-0.1008
-0.4	-0.2352	-0.2354	-0.2353	-0.2355
-0.2	-0.3421	-0.3422	-0.3422	-0.3426
0	-0.4213	-0.4213	-0.4213	-0.4213
0.2	-0.3421	-0.3422	-0.3422	-0.3426
0.4	-0.2352	-0.2354	-0.2353	-0.2355
0.6	-0.1008	-0.1006	-0.1008	-0.1008
0.8	-1.0000	-1.0000	-1.0000	-1.0000

Table 2: Comparison of present results with existing literature for $S_1 = 0.4$, $Re = 0.4$, $\alpha = 0.4$, $\beta = 0.3$, $Q = 0.6$, $x = 1$, $R_m = 2$.

.

6. CONCLUSIONS

In the present study, we have investigated the ciliary-induced magnetohydrodynamic copper-water nanofluid dissipative flow and heat transfer in a two-dimensional channel with magnetic induction and electrical field effects. The non-linear equations governing the conservation of mass, momentum, magnetic field and electrical field have been reduced to a system of coupled linearized partial differential equations via suitable coordinate and variable transformations, under the classical low Reynolds number (viscous-dominated) approximation. An appropriate elliptical path geometric model has been implemented for the cilia behavior. Magnetic Reynolds number has also been taken to be sufficiently high to generate magnetic induction effects. Numerical evaluation of the closed-form solutions for stream function, pressure rise, induced magnetic field function and temperature, has been conducted carefully via Mathematica symbolic software. The present study has shown that:

- Increasing Brinkman number (viscous dissipation parameter) elevates temperature in the regime, and also assists in the generation of closed loops i.e. thermal boluses in the isotherm distributions.

- The presence of nano-particles i.e. implementation of copper-water nanofluid always achieves higher temperatures than with the pure fluid.
- Increasing magnetic Reynolds number encourages the growth of bolus in the streamline distributions and furthermore weakly reduces current density magnitudes whereas it increases axial pressure gradient magnitudes. Furthermore greater magnetic Reynolds number elevates axial induced magnetic field in the lower channel half space, whereas it reduces it in upper channel half space. Additionally greater magnetic Reynolds number increases pressure rise for negative flow rates and reduces it for positive flow rates. Also temperature is reduced with greater magnetic Reynolds number and flow deceleration in the channel core (plug) flow region caused. However at the channel plates (boundaries) the flow is weakly accelerated with greater magnetic Reynolds numbers.
- Increasing Størmer magnetohydrodynamic number is found to reduce substantially the channel core region velocity magnitudes and to depress temperature in the core zone, although there is a weak increase in temperatures near both plates. Larger Stormer numbers (as with magnetic Reynolds number) tend to elevate pressure rise for negative flow rates and to reduce them with positive flow rates. Increasing Stormer number however has the opposite effect to magnetic Reynolds number on the axial induced magnetic field component, since it suppresses magnitudes in the lower channel half space, whereas it enhances values in the upper channel half space.
- Increasing electrical field parameter enhances the current density, as does an increase in magnetic Reynolds number. The copper nanofluid also achieves higher electrical current density values than the pure fluid. However greater Stormer numbers significantly suppress the electrical current density.
- Increasing flow rate is found to enhance pressure gradient and to depress temperatures.
- Increasing Reynolds number, enhances pressure gradient magnitudes and increases pressure rise for negative flow rate and reduces it for positive flow rate. The core flow region is decelerated with increasing Reynolds number whereas near the channel plates, a strong acceleration is generated in the axial flow.

The present computations are applicable to simulations of flow control in nano-magneto-biomimetic technologies. They have however neglected Hall current effects and these will be addressed in the near future.

REFERENCES

[1] M. Sleigh, Patterns of ciliary beating, Symposia of the Society for Experimental Biology, 1967, pp. 131-150.

[2] S. Gueron, and N. Liron, Ciliary motion modeling, and dynamic multicilia interactions. Biophysical journal 63 (1992) 1045.

[3] O.V. Salata, Applications of nanoparticles in biology and medicine. Journal of nanobiotechnology 2 (2004) 1.

[4] L. Zhang, F. Gu, J. Chan, A. Wang, R. Langer, and O. Farokhzad, Nanoparticles in medicine: therapeutic applications and developments. Clinical pharmacology and therapeutics 83 (2008) 761-769.

[5] N.S. Akbar, S. Nadeem, T. Hayat, and A.A. Hendi, Peristaltic flow of a nanofluid with slip effects. Meccanica 47 (2012) 1283-1294.

[6] D. Tripathi, and O.A. Bég, Mathematical Modelling of Peristaltic Pumping of Nano-Fluids. in: S.K. Basu, and N. Kumar, (Eds.), Modelling and Simulation of Diffusive Processes: Methods and Applications, Springer International Publishing, Cham, 2014, pp. 69-95.

[7] M. Mustafa, S. Hina, T. Hayat, and A. Alsaedi, Influence of wall properties on the peristaltic flow of a nanofluid: analytic and numerical solutions. International Journal of Heat and Mass Transfer 55 (2012) 4871-4877.

[8] O.A. Beg, M.J. UDDIN, and W. Khan, Bioconvective non-Newtonian nanofluid transport in porous media containing micro-organisms in a moving free stream. Journal of Mechanics in Medicine and Biology 15 (2015) 1550071.

[9] I. Anghel, and A.M. Grumezescu, Hybrid nanostructured coating for increased resistance of prosthetic devices to staphylococcal colonization. Nanoscale research letters 8 (2013) 1-6.

[10] A. Ebaid, and E.H. Aly, Exact analytical solution of the peristaltic nanofluids flow in an asymmetric channel with flexible walls and slip condition: application to the cancer treatment. Computational and mathematical methods in medicine 2013 (2013).

[11] N.S. Akbar, E. Maraj, and A.W. Butt, Copper nanoparticles impinging on a curved channel with compliant walls and peristalsis. The European Physical Journal Plus 129 (2014) 1-10.

[12] N. Saurín, T. Espinosa, J. Sanes, F.-J. Carrión, and M.-D. Bermúdez, Ionic Nanofluids in Tribology. Lubricants 3 (2015) 650-663.

[13] O.A. Bég, F. Mabood, and M. Nazrul Islam, Homotopy Simulation of Nonlinear Unsteady Rotating Nanofluid Flow from a Spinning Body. International Journal of Engineering Mathematics 2015 (2015).

[14] M.J. Uddin, M. Kabir, and O.A. Bég, Computational investigation of Stefan blowing and multiple-slip effects on buoyancy-driven bioconvection nanofluid flow with microorganisms. International Journal of Heat and Mass Transfer 95 (2016) 116-130.

[15] N.S. Akbar, and A.W. Butt, CNT suspended nanofluid analysis in a flexible tube with ciliated walls. The European Physical Journal Plus 129 (2014) 1-10.

[16] N. Sher Akbar, A. Wahid Butt, and N. Noor, Heat transfer analysis on transport of copper nanofluids due to metachronal waves of cilia. Current Nanoscience 10 (2014) 807-815.

[17] S. Munawar, A. Mehmood, and A. Ali, Time-dependent flow and heat transfer over a stretching cylinder. Chinese Journal of Physics 50 (2012) 828-848.

[18] S. Rahman, R. Ellahi, S. Nadeem, and Q.Z. Zia, Simultaneous effects of nanoparticles and slip on Jeffrey fluid through tapered artery with mild stenosis. Journal of Molecular Liquids 218 (2016) 484-493.

[19] M. Akbarzadeh, S. Rashidi, M. Bovand, and R. Ellahi, A sensitivity analysis on thermal and pumping power for the flow of nanofluid inside a wavy channel. Journal of Molecular Liquids 220 (2016) 1-13.

[20] R. Ellahi, M. Hassan, and A. Zeeshan, Shape effects of nanosize particles in Cu–H2O nanofluid on entropy generation. International Journal of Heat and Mass Transfer 81 (2015) 449-456.

[21] R. Ellahi, R. Ellahi, A. Zeeshan, A. Zeeshan and M. Hassan, Particle shape effects on Marangoni convection boundary layer flow of a nanofluid. International Journal of Numerical Methods for Heat & Fluid Flow 26 (2016) 2160-2174.
[22] N.S. Akbar, N. Kazmi, D. Tripathi, and N.A. Mir, Study of heat transfer on physiological driven movement with CNT nanofluids and variable viscosity. Computer Methods and Programs in Biomedicine 136 (2016) 21-29.
[23] A. Ito, M. Shinkai, H. Honda, and T. Kobayashi, Medical application of functionalized magnetic nanoparticles. Journal of bioscience and bioengineering 100 (2005) 1-11.
[24] D.-B. Shieh, F.-Y. Cheng, C.-H. Su, C.-S. Yeh, M.-T. Wu, Y.-N. Wu, C.-Y. Tsai, C.-L. Wu, D.-H. Chen, and C.-H. Chou, Aqueous dispersions of magnetite nanoparticles with NH 3+ surfaces for magnetic manipulations of biomolecules and MRI contrast agents. Biomaterials 26 (2005) 7183-7191.
[25] M. Sheikholeslami, M. Gorji-Bandpy, D. Ganji, S. Soleimani, and S. Seyyedi, Natural convection of nanofluids in an enclosure between a circular and a sinusoidal cylinder in the presence of magnetic field. International Communications in Heat and Mass Transfer 39 (2012) 1435-1443.
[26] M. Sheikholeslami, and R. Ellahi, Three dimensional mesoscopic simulation of magnetic field effect on natural convection of nanofluid. International Journal of Heat and Mass Transfer 89 (2015) 799-808.
[27] M. Akbarzadeh, S. Rashidi, M. Bovand and R. Ellahi**,** A sensitivity analysis on thermal and pumping power for the flow of nanofluid inside a wavy channel**,** Journal of Molecular Liquids. *220* , (2016)*1-13.*
[28] R. Ellahi, M. Hassan, A. Zeeshan , A. A. Khan AAShape effects of nanoparticles suspended in HFE-7100 over wedge with entropy generation and mixed convection. Appl Nanosci, 6(5) (2016) 641-651.
[29] A. Zeeshan, A. Majeed, R. Ellahi, Effect of magnetic dipole on viscous ferro-fluid past a stretching surface with thermal radiation, *Journal of Molecular Liquids, 215*(2016)*549-554*.
[30] M. Ferdows, M.S. Khan, O.A. Bég, M. Azad, and M. Alam, Numerical study of transient magnetohydrodynamic radiative free convection nanofluid flow from a stretching permeable surface. Proceedings of the Institution of Mechanical Engineers, Part E: Journal of Process Mechanical Engineering 228 (2014) 181-196.
[31] V. Roberts, Magnetohydrodynamic pumping of blood. Medical and biological engineering 10 (1972) 57-59.
[32] O.A. Bég, A. Bakier, V. Prasad, J. Zueco, and S. Ghosh, Nonsimilar, laminar, steady, electrically-conducting forced convection liquid metal boundary layer flow with induced magnetic field effects. International Journal of Thermal Sciences 48 (2009) 1596-1606.
[33] S. Ghosh, O.A. Bég, and J. Zueco, Hydromagnetic free convection flow with induced magnetic field effects. Meccanica 45 (2010) 175-185.
[34] S. Ghosh, O.A. Bég, J. Zueco, and V. Prasad, Transient hydromagnetic flow in a rotating channel permeated by an inclined magnetic field with magnetic induction and Maxwell displacement current effects. Zeitschrift für angewandte Mathematik und Physik 61 (2010) 147-169.
[35] J. Zueco, and O.A. Bég, Network numerical analysis of hydromagnetic squeeze film flow dynamics between two parallel rotating disks with induced magnetic field effects. Tribology International 43 (2010) 532-543.
[36] R. Bhargava, O.A. Bég, S. Sharma, and J. Zueco, Finite element study of nonlinear two-dimensional deoxygenated biomagnetic micropolar flow. Communications in Nonlinear Science and Numerical Simulation 15 (2010) 1210-1223.
[37] O.A. Bég, M. Ferdows, S. Shamima, and M.N. Islam, Numerical simulation of Marangoni magnetohydrodynamic bio-nanofluid convection from a non-isothermal surface with magnetic induction effects: a bio-nanomaterial manufacturing transport model. Journal of Mechanics in Medicine and Biology 14 (2014) 1450039.
[38] O.A. Bég, D. Tripathi, T. Sochi, and P. Gupta, Adomian Decomposition Method (ADM) simulation of magneto-bio-tribological squeeze film with magnetic induction effects. Journal of Mechanics in Medicine and Biology 15 (2015) 1550072.

[39] K.S. Mekheimer, Peristaltic flow of a magneto-micropolar fluid: effect of induced magnetic field. Journal of Applied Mathematics 2008 (2008).
[40] K.S. Mekheimer, Effect of the induced magnetic field on peristaltic flow of a couple stress fluid. Physics Letters A 372 (2008) 4271-4278.
[41] T. Hayat, N. Saleem, and N. Ali, Effect of induced magnetic field on peristaltic transport of a Carreau fluid. Communications in Nonlinear Science and Numerical Simulation 15 (2010) 2407-2423.
[42] T. Hayat, S. Noreen, M.S. Alhothuali, S. Asghar, and A. Alhomaidan, Peristaltic flow under the effects of an induced magnetic field and heat and mass transfer. International Journal of Heat and Mass Transfer 55 (2012) 443-452.
[43] A. Bejan, Convection heat transfer, John wiley & sons, 2013.
[44] R. Subba, and R. Gorla, Entropy generation in thermally fully developed electro-osmotic flow in circular microtubes. International Journal of Microscale and Nanoscale Thermal and Fluid Transport Phenomena 5 (2014) 279.